IOPscience iopscience.iop.org

Home Search Collections Journals About Contact us My IOPscience

Magnetic and caloric properties of magnetic nanoparticles: an equilibrium study

This article has been downloaded from IOPscience. Please scroll down to see the full text article.

2006 J. Phys.: Condens. Matter 18 11309

(http://iopscience.iop.org/0953-8984/18/49/022)

View the table of contents for this issue, or go to the journal homepage for more

Download details:
IP Address: 129.252.86.83
The article was downloaded on 28/05/2010 at 14:52

Please note that terms and conditions apply.

INSTITUTE OF PHYSICS PUBLISHING JOURNAL OF PHYSICS: CONDENSED MATTER

J. Phys.: Condens. Matter **18** (2006) 11309–11322 doi:10.1088/0953-8984/18/49/022

Magnetic and caloric properties of magnetic nanoparticles: an equilibrium study

Malay Bandyopadhyay and Jayee Bhattacharya[1]

S N Bose National Centre for Basic Sciences, JD Block, Sector III, Salt Lake City, Kolkata 700098, India

E-mail: malay@bose.res.in and jayee@bose.res.in

Received 28 August 2006, in final form 30 October 2006
Published 22 November 2006
Online at stacks.iop.org/JPhysCM/18/11309

Abstract

The static or thermal equilibrium properties of non-interacting magnetically anisotropic nanoparticles are studied in the framework of classical theory. Various important thermal equilibrium properties, e.g. internal energy, specific heat, magnetization and susceptibility, are derived from basic thermodynamic functions such as the partition function and thermodynamic potentials. The central issue in this paper is to study the effect of anisotropic potential on these thermal equilibrium properties. We extensively study the linear and nonlinear susceptibilities and their temperature dependence. We also give a comparative study of the magnetic properties of a superparamagnetic fine particle system and a canonical spin-glass system and thus invoke the similarities and differences between the two.

(Some figures in this article are in colour only in the electronic version)

1. Introduction

Since the pioneering work of Néel five decades ago [1], the magnetic properties of nanoparticles have attracted immense attention due to their significance in both technological applications and fundamental research [2–6]. These systems can be considered as very good model systems for rotational Brownian motion, thermally activated multistable systems [7] and stochastic resonance [8].

The magnetic moment of a nanoparticle consists of a single domain structure of ferromagnetic spins with a large net spin ($S \sim 10^3$–10^4, supermoment). This spin is coupled to the environmental degrees of freedom of the host material. Due to dynamic disturbances of the surroundings, this large spin undergoes a rotational Brownian motion surmounting the magnetic anisotropy potential barrier [1, 9]. In the high barrier limit, the magnetic response of non-interacting single domain particles will follow the Néel [1] relaxation process characterized

[1] Author to whom any correspondence should be addressed.

 © 2006 IOP Publishing Ltd Printed in the UK

by the relaxation time

$$\tau = \tau_0 \exp\left(\frac{\Delta E_a}{k_B T}\right) \tag{1}$$

where $\tau_0 \simeq 10^{-10}$–10^{-13} s and is related to intrawell motion, the height of the energy barrier due to anisotropy $\Delta E_a = KV$ (K is the anisotropy constant and V is the particle volume), k_B is the Boltzmann constant and T denotes absolute temperature. Now depending on the relation between the relaxation time τ and the measurement time t_m, different phenomena are observed. When $\tau \ll t_m$, the magnetic moment exhibits the thermal equilibrium distribution as in a paramagnet. Due to the large value of S, the term superparamagnet is used. On the other hand, if $\tau \gg t_m$, the reversal mechanism is blocked and the magnetic moment stays very close to the energy minimum. Under an intermediate condition ($\tau \sim t_m$) there are non-equilibrium phenomena, e.g. magnetic relaxation.

The subject of spin-glass freezing of many disordered magnetic materials at low temperature is an old one [10–13]. The analogy between the macroscopic behaviour of certain magnetic 'glassy' systems (e.g. Au–Fe alloy) and that of ensembles of fine nanomagnetic particles is an enigmatic subject and has received recurrent attention during the last few years [14–17]. However, it is not clear whether all the magnetic properties of fine-particle systems are same as those of typical spin-glasses (e.g. Au–Fe alloys). The nature of spin-glass freezing is still controversial. So detailed studies of magnetic properties of fine particles is necessary in order to clarify whether spin-glass freezing is the progressive freezing of the super-moments.

The spin-glass transition is characterized by the critical behaviour of nonlinear magnetic susceptibilities (NLMS), and in this respect it plays a significant role. Bitoh *et al* have shown $\chi_{2n}(\omega, T)$ to be a suitable experimental tool for distinguishing between a spin-glass and a fine-particle system. The remarkable feature is the nature of the decrease of χ_{2n} as T increases above the peak temperature. Unfortunately, theoretical descriptions of NLMS of non-interacting fine particles are very rare [18, 19]. The first theoretical description on NLMS was given by Jonson *et al* [18] and later extended by Garcia-Palacios *et al* [19].

In this paper we derive rigorous expressions for the static thermal equilibrium properties of non-interacting magnetically anisotropic nanoparticles in the framework of classical physics. The purpose of this paper is to gain a deeper insight into the thermal equilibrium properties of non-interacting anisotropic fine-particle systems.

With the preceding background, we organize our paper as follows. In the next section we discuss the effective Hamiltonian of an anisotropic nanoparticle and then derive some basic thermodynamic functions. Section 3 is devoted to the study of magnetization, linear susceptibility and nonlinear susceptibilities. In section 4 we study the caloric quantities, i.e. internal energy, entropy and specific heat. The central issue is to study the effect of the magnetic anisotropy on the magnetization susceptibilities as well as on the caloric quantities and to invoke the differences between the spin-glass transition and the progressive freezing of the supermoments. We summarize our results and conclude in section 5.

2. Effective Hamiltonian and partition function

We mainly consider systems where the magnetic anisotropy energy has the simplest axial symmetry. When an external field $\vec{B}$ is applied the total magnetic energy is

$$\mathcal{H}(\vec{m}) = -\frac{KV}{m^2}(\vec{m}\cdot\hat{n})^2 - \vec{m}\cdot\vec{B}, \tag{2}$$

where $\hat{n}$ is a unit vector along the anisotropy axis. Introducing the unit vectors $\hat{e}$ in the direction

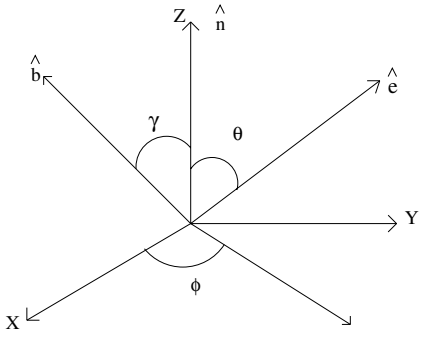

Figure 1. Coordinate system showing the unit vectors $\hat{e}$, $\hat{b}$ and $\hat{n}$ along with the angles referred to.

of the magnetic moment, $\vec{m}$ ($\hat{e} = \frac{\vec{m}}{m}$), $\hat{b}$ in the direction of the magnetic field ($\hat{b} = \frac{\vec{B}}{B}$) (c.f. figure 1) and dimensionless anisotropy and field parameters $\sigma = \frac{KV}{k_B T}$ and $\xi = \frac{mB}{k_B T}$ one can express equation (2) as

$$-\beta\mathcal{H} = \sigma\left(\hat{e}\cdot\hat{n}\right)^2 + \xi\left(\hat{e}\cdot\hat{b}\right). \tag{3}$$

We choose the anisotropy axis $\hat{n}$ as the polar axis of a spherical coordinate system. (θ, ϕ) and $(\gamma, 0)$ denote the angular coordinates of $\hat{e}$ and $\hat{b}$, respectively. Then the total magnetic potential is given by

$$-\beta\mathcal{H} = \sigma\cos^2\theta + \xi_\parallel\cos\theta + \xi_\perp\sin\theta\cos\phi, \tag{4}$$

where $\xi_\parallel = \xi\cos\gamma$ and $\xi_\perp = \xi\sin\gamma$. The partition function associated with the Hamiltonian (cf equation (4)) is defined as

$$\mathcal{Z} = \int_0^\pi \mathrm{d}\theta\sin\theta\exp(\sigma\cos^2\theta + \xi_\parallel\cos\theta)I_0(\xi_\perp\sin\theta), \tag{5}$$

where $I_0(y)$ is a zeroth order modified Bessel function of the first kind [20]. After some algebra one can show

$$\mathcal{Z} = 2R(\sigma)\sum_{i=0}^{\infty}\frac{C_i(\sigma,\gamma)}{i!}\xi^{2i}, \tag{6}$$

where

$$C_i(\sigma,\gamma) = i!\sum_{k=0}^{i} b_{i-k,k}(\gamma)\sum_{m=0}^{k}(-1)^m\frac{k!}{m!(k-m)!}\frac{R^{(i-k+m)}(\sigma)}{R(\sigma)}. \tag{7}$$

$$b_{i,k}(\gamma) = \frac{1}{(2i)!2^{2k}(k!)^2}\cos^{2i}\gamma\sin^{2k}\gamma, \tag{8}$$

and

$$R^{(l)}(\sigma) = \int_0^1 \mathrm{d}z\, z^{2l}\exp(\sigma z^2). \tag{9}$$

The partition function hence obtained helps the further calculation of the equilibrium properties.

3. Equilibrium properties

In this section we discuss a number of important thermodynamic quantities of non-interacting magnetic nanoparticles with axially symmetric magnetic anisotropy. In particular, we analyse the effect of magnetic anisotropy on the magnetization ($\mathcal{M}$) as well as the linear (χ_0) and nonlinear (χ_2, χ_4) susceptibilities. The differences and similarities of the linear and nonlinear susceptibilities between canonical spin-glass systems, such as $Au_{96}Fe_4$ [21–23], and magnetic nanoparticle systems, such as $Cu_{97}Co_3$ [17], are presented.

3.1. Magnetization

The magnetization along the external field direction for classical spins with axially symmetric magnetic anisotropy is defined as follows:

$$\mathcal{M}_B = \langle \vec{m} \cdot \hat{b} \rangle_{\text{eq}} = m \frac{\partial}{\partial \xi} (\ln \mathcal{Z}). \tag{10}$$

Taking derivative w.r.t. ξ of the low-ξ expansion of $\ln \mathcal{Z}$, we obtain

$$\mathcal{M}_B = m[2C_1\xi + 2(C_2 - C_1^2)\xi^3 + (C_3 - 3C_2C_1 + 2C_1^3)\xi^5 + \cdots] \tag{11}$$

where the coefficients C_i are given by equation (7). We now study equation (11) for particular cases.

(i) *Isotropic case* ($\sigma = 0$). In this case $C_1 = \frac{1}{6}$, $C_2 = \frac{1}{60}$, $C_3 = \frac{1}{840} \ldots$ and so on. Thus we obtain

$$\mathcal{M}_{B,\text{Lan}} = mL(\xi), \tag{12}$$

where $L(\xi)$ is the Langevin function.

(ii) *Ising case* ($\sigma \to \infty$). In this regime $C_1 = \frac{\cos^2\gamma}{2}$, $C_2 = \frac{\cos^4\gamma}{12}$, $C_3 = \frac{\cos^6\gamma}{120}$ and so on. Thus the magnetization becomes

$$\mathcal{M}_{B,\text{Ising}} = m \cos\gamma \tanh \xi_{\parallel}. \tag{13}$$

This shows that magnetization vanishes when $\vec{B}$ is perpendicular to the anisotropy axis $\hat{n}$.

(iii) *Plane-rotator case* ($\sigma \to -\infty$). In this case $C_1 = \frac{\sin\gamma}{4}$, $C_2 = \frac{\sin^4\gamma}{32}$, $C_3 = \frac{\sin^6\gamma}{384}$ and so on.

$$\mathcal{M}_{B,\text{rot}} = m \sin\gamma \frac{I_1(\xi_\perp)}{I_0(\perp)}. \tag{14}$$

In this case magnetization vanishes when $\vec{B}$ is perpendicular to the rotator plane.

(iv) *Longitudinal field case* ($\vec{B} \parallel \hat{n}$). Now we have $C_1 = \frac{R'}{2R}$; $C_2 = \frac{R''}{12R}$; $C_3 = \frac{R'''}{120R}$ and so on. Now the magnetization becomes

$$\mathcal{M}_{B,\parallel} = m \left[\frac{R'}{R}\xi + \frac{1}{2}\left(\frac{1}{3}\frac{R''}{R} - \left(\frac{R'}{R}\right)^2 \right) \xi^3 + \cdots \right]. \tag{15}$$

Here one can easily note that $\mathcal{M}_B$ depends on B and T through ξ in the first three cases. So the magnetization versus $\frac{B}{T}(\sim\xi)$ curves corresponding to different temperatures collapse onto a single master curve as shown in figure 2(a). However, outside these three limiting cases, T does not enter in $\mathcal{M}_B$ via $\frac{B}{T}$ only, but $\mathcal{M}_B$ depends on ξ as well as σ. This is shown in figure 2(b) for the longitudinal field case. As T decreases, one can see the crossover from the high-temperature isotropic regime to the low-temperature Ising regime. This crossover is induced by the magnetic anisotropy.

3.2. Linear susceptibility (χ_0)

We now study the linear susceptibility of classical 'superspin' with axially symmetric magnetic anisotropy. We start our discussion with the low-field expansion of the magnetization ($H = \frac{B}{\mu_0}$)

$$\mathcal{M}_B = \chi_0 H + \chi_2 H^3 + \chi_4 H^5 + \ldots, \tag{16}$$

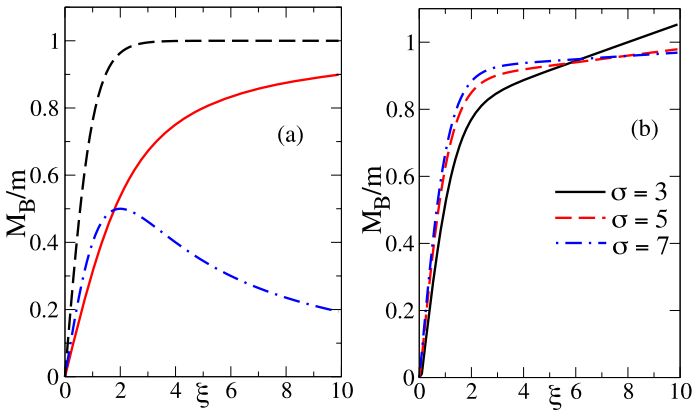

Figure 2. (a) Magnetization versus field curves corresponding to different temperatures for the isotropic case (red, solid line), for the Ising case (black, dashed line) and for the plane-rotator case (blue, dot-dashed line). (b) Magnetization versus longitudinal field showing the non-$\frac{B}{T}$ superposition of the magnetization curves for three different values of σ.

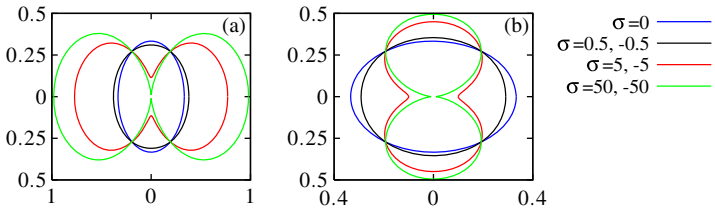

Figure 3. Polar plot of χ_0 versus γ for different values of σ: (a) easy-axis anisotropy, (b) easy-plane anisotropy.

where χ_0 is the linear susceptibility and χ_2, χ_4 are the nonlinear susceptibilities. Comparing equations (11) and (16) we obtain

$$\chi_0 = 2mC_1 = \frac{\mu_0 m^2}{k_B T} 2C_1(\sigma, \gamma). \tag{17}$$

Thus the general expression of linear susceptibility is given by

$$\chi_0 = \chi_0^{\parallel} \cos^2\gamma + \chi_0^{\perp} \sin^2\gamma, \tag{18}$$

where $\chi_0^{\parallel} = \frac{\mu_0 m^2}{k_B T}\frac{R'}{R}$; $\chi_0^{\perp} = \frac{\mu_0 m^2}{k_B T}\frac{R-R'}{2R}$. Figure 3 shows a polar plot of linear susceptibility as a function of the angle between the anisotropy axis and the probing field for the easy-axis anisotropy and easy-plane anisotropy for various values of σ. It shows that the larger $|\sigma|$ is, the more anisotropic the χ_0 curves become. The limiting cases of the linear susceptibility for the four regimes are $\chi_0^{\text{Lan}} = \frac{\mu_0 m^2}{3k_B T}$, $\chi_0^{\text{Ising}} = \frac{\mu_0 m^2}{k_B T}\cos^2\gamma$, $\chi_0^{\text{Plane-Rotator}} = \frac{\mu_0 m^2}{2k_B T}\sin^2\gamma$ and $\chi_0^{\parallel} = \frac{\mu_0 m^2}{k_B T}\frac{R'}{R}$. In figure 4(a) we plot the reduced linear susceptibility versus the dimensionless anisotropy parameter in the longitudinal and transverse field cases. Both curves coincide at $\sigma = 0$ taking the Langevin value of $\frac{1}{3}$. It is understood from figure 4(a) that the longitudinal and transverse field cases interchange their roles when the sign of the anisotropy is changed. Figure 4(b) shows a log–log plot of the linear susceptibility versus the dimensionless temperature ($\frac{1}{\sigma}$). As the influence of the anisotropy decreases with increasing temperature, χ_0 undergoes a smooth crossover from the low-temperature Ising regime to the high-temperature

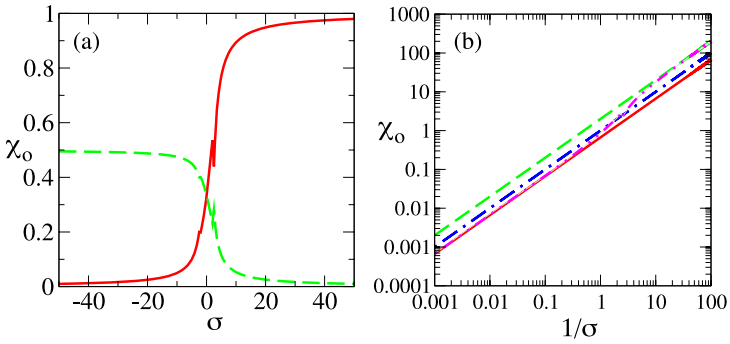

Figure 4. (a) Plot of linear susceptibility versus σ in the longitudinal (red, solid line) and transverse (green, dashed line) field cases. (b) Log–log plot of χ_0 versus $\frac{1}{\sigma}$ for the isotropic case (red, solid line), Ising case (green, dashed line), plane-rotator case (blue, dot-dashed line) and the randomly distributed anisotropy case (magenta, double dot-dashed line).

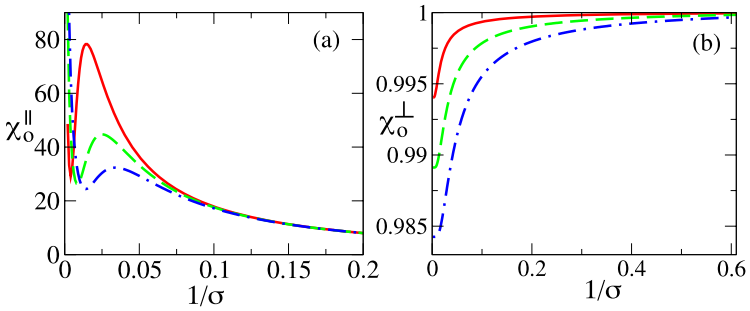

Figure 5. (a) Longitudinal and (b) transverse components of the linear susceptibility versus $1/\sigma$ with $h = 0.006$ (red, solid line), $h = 0.011$ (green, dashed line) and $h = 0.016$ (blue, dot-dashed line) and these curves exhibit spin-glass like maximum.

Langevin case. The slope of the curves is as occurs in the asymptotic regime (T^{-1}) dependence, but deviation from this inverse temperature dependence is sizable in the transitional region. In this transitional region the slope is less than 1. The temperature dependence of the longitudinal and transverse component of the linear susceptibility seem to have broad peaks (figures 5(a), (b)). Both $\chi_0^{\parallel}$ and $\chi_0^{\perp}$ show a broad peak. Bitoh *et al* [17, 24] have shown temperature dependence of χ_0 in a $Cu_{97}Co_3$ fine-particle system and in a $Au_{96}Fe_4$ spin-glass system. The peak of $Cu_{97}Co_3$ is broad compared to that of $Au_{96}Fe_4$. So our theoretical results (figure 5) qualitatively reproduce the experimental results.

3.3. Nonlinear susceptibilities (χ_2, χ_4)

We now study the nonlinear susceptibilities of classical spins with uniaxial magnetic anisotropy. The main goal of this study is to invoke the suitability of these quantities for the study of collective phenomena of glassy systems and also the glassy like behaviour of some fine particles ($Cu_{97}Co_3$). Bitoh *et al* [17, 24] have shown that χ_2 gives the key to clarifying the differences between the spin-glass transition and the progressive freezing of the supermoments. In this subsection we present a rigorous theoretical analysis of these nonlinear magnetic susceptibilities and discuss their different properties for the classical spins as well as for the spin-glass system.

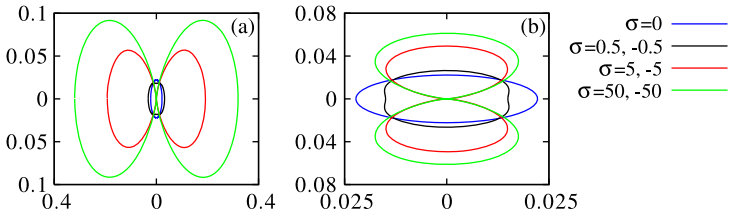

Figure 6. Polar plot of χ_2 versus γ for different values of σ: (a) easy-axis anisotropy, (b) easy-plane anisotropy.

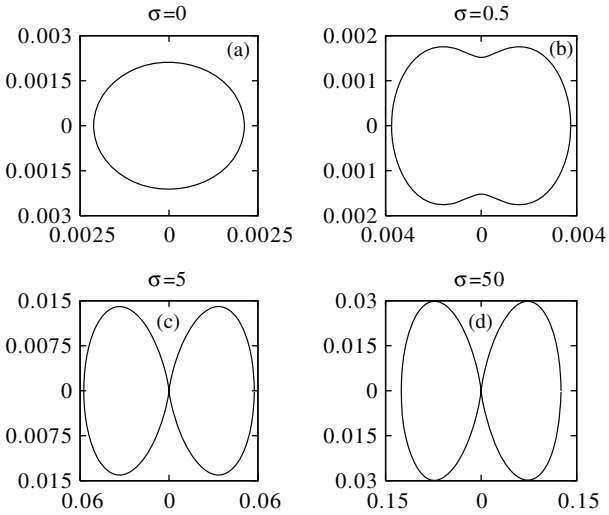

Figure 7. Polar plot of χ_4 versus γ for different values of σ for easy-axis anisotropy.

The nonlinear susceptibilities are defined as the coefficients of the nonlinear terms in the expansion of the magnetization in powers of the external field. Now comparing equations (11) and (16) we obtain

$$\chi_2 = \frac{\mu_0^3 m^4}{(k_B T)^3} 2\left(C_2 - C_1^2\right), \tag{19}$$

$$\chi_4 = \frac{\mu_0^5 m^6}{(k_B T)^5}\left(C_3 - 3C_2C_1 + 2C_1^3\right). \tag{20}$$

In figure 6 we plot the angular dependence of the reduced nonlinear susceptibility χ_2 in the cases of easy-axis anisotropy and easy-plane anisotropy for various values of σ. It is seen that χ_2 curves become more anisotropic as $|\sigma|$ increases and become quite different from circles for $|\sigma| > 0$. The size of the isotropic case is different for the $K > 0$ and $K < 0$ cases because the maximum values of χ_2 for $K > 0$ and $K < 0$ are quite different. Figures 7 and 8 display the angular dependence of χ_4 for the $K > 0$ and $K < 0$ cases, respectively. Let us consider various particular cases for the nonlinear susceptibilities.

(i) *Isotropic case* ($\sigma = 0$):

$$\chi_2 = -\frac{\mu_0^3 m^4}{45(k_B T)^3} \tag{21}$$

$$\chi_4 = \frac{2}{945}\frac{\mu_0^5 m^6}{(k_B T)^5}. \tag{22}$$

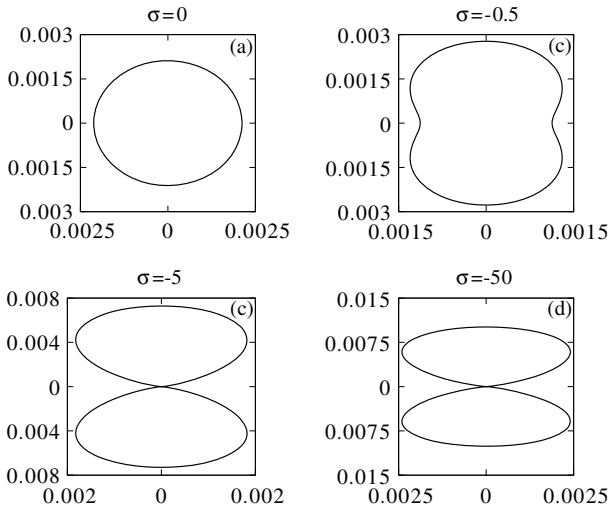

Figure 8. Polar plot of χ_4 versus γ for different values of σ for easy-plane anisotropy.

(ii) *Ising case* ($\sigma \to \infty$):

$$\chi_2 = -\frac{\mu_0^3 m^4}{3(k_B T)^3} \cos^4 \gamma \tag{23}$$

$$\chi_4 = \frac{2}{15} \frac{\mu_0^5 m^6}{(k_B T)^5} \cos^6 \gamma. \tag{24}$$

(iii) *Plane-rotator case* ($\sigma \to -\infty$):

$$\chi_2 = -\frac{\mu_0^3 m^4}{16(k_B T)^3} \sin^4 \gamma \tag{25}$$

$$\chi_4 = \frac{1}{96} \frac{\mu_0^5 m^6}{(k_B T)^5} \sin^6 \gamma. \tag{26}$$

(iv) *Longitudinal field case* ($\vec{b} \parallel \hat{n}$):

$$\chi_2 = \frac{\mu_0^3 m^4}{(k_B T)^3} \left[\frac{1}{2} \left(\frac{1}{3} \frac{R''}{R} - \left(\frac{R'}{R} \right)^2 \right) \right] \tag{27}$$

$$\chi_4 = \frac{\mu_0^5 m^6}{(k_B T)^5} \left[\frac{1}{4} \left(\frac{R'''}{30R} - \frac{R'' R'}{2R^2} + \left(\frac{R'}{R} \right)^3 \right) \right]. \tag{28}$$

Figure 9(a) shows χ_2 versus σ in the longitudinal and transverse field cases as well as for the anisotropy axes distributed at random. These three curves coincide at $\sigma = 0$ and take the Langevin value $-\frac{1}{45}$. A large deviation for the anisotropy is observed in the parallel field case. This deviation is dramatically reduced for a random distribution of anisotropy axes. The longitudinal and the transverse field cases interchange their roles when the sign of the anisotropy is reversed. In figure 9(b) we show the log–log plot of χ_2 versus $\frac{1}{\sigma}$ for the Ising case, plane-rotator case, isotropic case and for the random distribution of anisotropy axes. We can see a smooth crossover from the low-temperature Ising regime to the high-temperature isotropic regime. In the transitional regime the departure of $\chi_2(T)$ from an inverse temperature-cubed law is sizable. Figure 10(a) shows the log–log plot of χ_4 versus dimensionless temperature for different limiting cases like Ising, isotropic, plane-rotator and the randomly oriented anisotropy axes. It is seen that as the influence

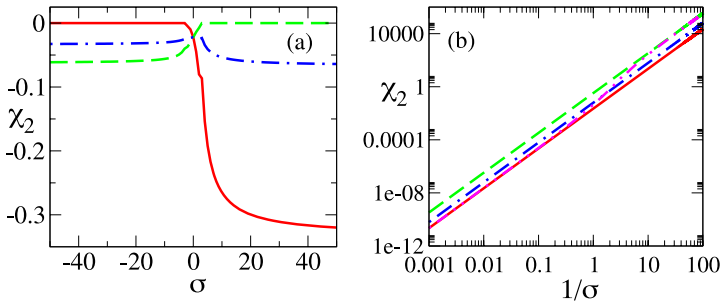

Figure 9. (a) Plot of χ_2 versus σ in the longitudinal (red, solid line), transverse (green, dashed line) field and random distribution (blue, dot-dashed line) cases. (b) Log–log plot of χ_2 versus $\frac{1}{\sigma}$ for the isotropic case (red, solid line), Ising case (green, dashed line), plane-rotator case (blue, dot-dashed line) and the randomly distributed anisotropy case (magenta, double dot-dashed line).

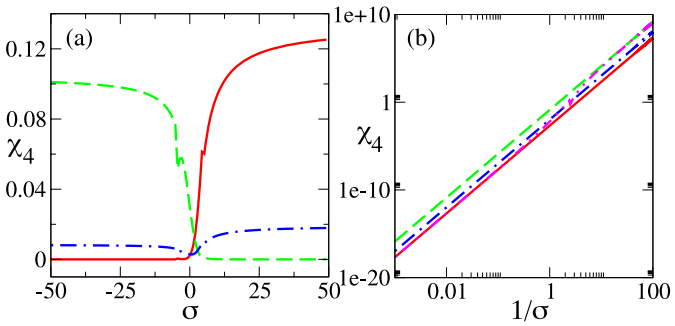

Figure 10. (a) Plot of χ_4 versus σ in the longitudinal (red, solid line), transverse (green, dashed line) field and random distribution (blue, dot-dashed line) cases. (b) Log–log plot of χ_4 versus $\frac{1}{\sigma}$ for the isotropic case (red, solid line), Ising case (green, dashed line), plane-rotator case (blue, dot-dashed line) and the randomly distributed anisotropy case (magenta, double dot-dashed line).

of anisotropy decreases with increasing T, χ_4 goes smoothly from the high-temperature isotropic regime to the low-temperature Ising regime. The transition region is very wide in range, and in the transition region there is a significant deviation from the T^{-5} law. On the other hand, figure 10(b) shows χ_4 versus σ in the longitudinal, transverse and random distributed anisotropy axes cases. The three curves coincide at $\sigma = 0$ and they take the Langevin value $\frac{2}{945}$. Although the large deviation from the Langevin result is observed in the parallel field case, the deviation in the perpendicular field case is comparable to that of the parallel case. The random distribution of anisotropy axes reduces this anisotropy induced departure. One can notice that qualitatively the nature of $\chi_4^{\parallel}$ and $\chi_4^{\perp}$ are just opposite to that of $\chi_2^{\parallel}$ and $\chi_2^{\perp}$. Again the roles of the longitudinal and the transverse field cases are interchanged when the sign of the anisotropy is reversed.

Now we discuss about the canonical spin-glass phase transition based on the mean field theory. The first attempt to make a mean field theory of spin-glasses was made by Edwards and Anderson [10]. The Hamiltonian for the system is

$$\mathcal{H} = -\tfrac{1}{2}\sum_{\langle ij\rangle} J_{ij}\vec{S}_i \cdot \vec{S}_j - H\sum_i S_i^z, \tag{29}$$

where $\vec{S}_i$ is the spin vector on site i and S_i^z is the component of $\vec{S}_i$ along the applied field H.

The exchange coupling constants J_{ij} are randomly chosen according to a fixed distribution

$$p(J_{ij}) = \frac{1}{\sqrt{2\pi}\,J_0} \exp\left[-\frac{-(J_{ij}-J)^2}{2J_0^2}\right], \tag{30}$$

where J is a mean value and J_0 is a variance of the distribution. Following Suzuki *et al* [25] one can show that the order parameter susceptibility is

$$\chi_{\rm sg} \simeq \frac{1}{2k_{\rm B}^2 T_{\rm g}^2}\left(\frac{T_{\rm g}}{T-T_{\rm g}}\right), \tag{31}$$

where the spin-glass transition temperature $T_{\rm g}$ is $\frac{\sqrt{z}J_0}{k_{\rm B}}$. z is the number of nearest neighbour spins. Now following Wada *et al* [26] and Sherrington *et al* [27] we obtain for the linear susceptibility $\chi_0 \sim (\chi_{\rm sg})^{\frac{1}{2}}$. Thus

$$\chi_0 = \frac{1}{\sqrt{2k_{\rm B}^2 T_{\rm g}^2}}\left(\frac{T_{\rm g}}{T-T_{\rm g}}\right)^{\frac{1}{2}}. \tag{32}$$

The nonlinear susceptibilities χ_2 and χ_4 are given by

$$\chi_2 = -\frac{1}{2k_{\rm B}^3 T_{\rm g}^3}\left(\frac{T_{\rm g}}{T-T_{\rm g}}\right) \tag{33}$$

$$\chi_4 = \frac{1}{32k_{\rm B}^5 T_{\rm g}^5}\left(\frac{T_{\rm g}}{T-T_{\rm g}}\right)^{\frac{3}{2}}. \tag{34}$$

Thus both the linear and nonlinear susceptibilities of canonical spin-glass systems diverge at $T_{\rm g}$ obeying equations (32)–(34). χ_0 and χ_4 diverge positively whereas χ_2 diverges negatively at $T_{\rm g}$. On the other hand we have seen that both the linear susceptibility and χ_4 show a broad positive peak and χ_2 has a negative broad peak. The temperature dependence of χ_0, χ_2 and χ_4 are quite different for the classical superspins and that of the canonical spin-glass systems.

4. Caloric properties

In this section we discuss the caloric quantities like energy, entropy and specific heat in a number of particular situations.

(i) *Isotropic case* ($\sigma = 0$). In this case the internal energy is

$$u_{\rm Lan} = -m\left(\coth\xi - \frac{1}{\xi}\right). \tag{35}$$

The entropy is formulated as

$$\frac{S_{\rm Lan}}{k_{\rm B}} = \ln\left(\frac{2\sinh\xi}{\xi}\right) - \xi\left(\coth\xi - \frac{1}{\xi}\right). \tag{36}$$

The Langevin specific heat is given by

$$\frac{C_{B,\rm Lan}}{k_{\rm B}} = 1 - \frac{\xi^2}{\sinh^2\xi}. \tag{37}$$

(ii) *Zero field case*. In this case the mean energy is given by

$$u_{\rm unb} = -K\,v\frac{R'}{R}. \tag{38}$$

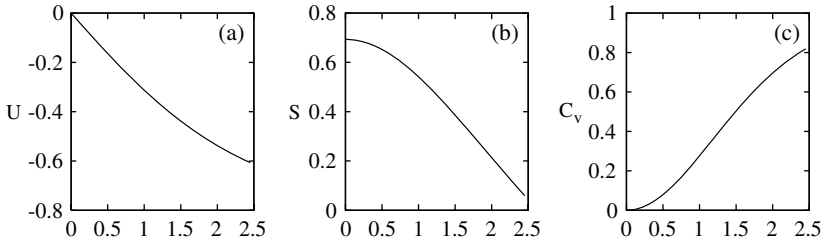

Figure 11. Inverse temperature dependence of (a) u, (b) S and (c) specific heat for the isotropic case.

Zero field entropy and specific heat are given by

$$\frac{S_{\rm unb}}{k_{\rm B}} = \ln(2R) - \sigma\frac{R'}{R}, \tag{39}$$

$$\frac{c_{B,\rm unb}}{k_{\rm B}} = \sigma^2\left[\frac{R''}{R} - \left(\frac{R'}{R}\right)^2\right]. \tag{40}$$

(iii) *Ising case* ($\sigma \to \infty$). In the Ising regime internal energy and entropy are given by

$$u_{\rm Ising} = -\left[Kv - \frac{Kv}{\sigma} + mB\cos\gamma\tanh\xi_{\parallel}\right] \tag{41}$$

$$\frac{S_{\rm Ising}}{k_{\rm B}} = \sigma - \ln\sigma + \ln(\cosh\xi_{\parallel}) - \beta\left(Kv - \frac{Kv}{\sigma} + mB\cos\gamma\tanh\xi_{\parallel}\right). \tag{42}$$

and the specific heat is

$$\frac{c_{\rm B,Ising}}{k_{\rm B}} = 1 + \xi^2\cos^2\gamma\,\mathrm{sech}^2(\xi\cos\gamma) - \xi\cos\gamma\tanh(\xi\cos\gamma). \tag{43}$$

(iv) *Plane-rotator case* ($\sigma \to -\infty$). In this limiting condition internal energy, entropy and specific heat are given by

$$u_{\rm rot} = \frac{Kv}{2\sigma} - \frac{I_1(\xi_\perp)}{I_0(\xi_\perp)}mB\sin\gamma, \tag{44}$$

$$\frac{S_{\rm rot}}{k_{\rm B}} = -\frac{1}{2} + \frac{\xi_\perp I_1(\xi_\perp)}{I_0(\xi_\perp)}, \tag{45}$$

$$\frac{c_{\rm B,rot}}{k_{\rm B}} = -\frac{1}{2} - \xi_\perp^2\left[\frac{I_0(\xi_\perp)I_2(\xi_\perp) - I_1^2(\xi_\perp)}{I_0^2(\xi_\perp)}\right]. \tag{46}$$

(v) *Longitudinal field case*. In this case internal energy is given by

$$u_{\parallel} = Kv\left[h^2 - \frac{(1+h)^3R'(\sigma_+) + (1-h)^3R'(\sigma_-)}{(1+h)R'(\sigma_+) + (1-h)R'(\sigma_-)}\right], \tag{47}$$

where $\sigma_\pm = \sigma(1\pm h)^2$ and $h = \frac{\xi}{2\sigma}$. The entropy and specific heat are given by

$$S_{\parallel} = \ln\left[(1+h)R(\sigma_+) + (1-h)R(\sigma_-)\right] - \sigma\frac{(1+h)^3R'(\sigma_+) + (1-h)^3R'(\sigma_-)}{(1+h)R'(\sigma_+) + (1-h)R'(\sigma_-)} \tag{48}$$

$$\frac{c_{B,\parallel}}{k_{\rm B}} = \left\{\frac{(1+h)^5R'(\sigma_+) + (1-h)^5R'(\sigma_-)}{(1+h)R'(\sigma_+) + (1-h)R'(\sigma_-)} - \left[\frac{(1+h)^3R'(\sigma_+) + (1-h)^3R'(\sigma_-)}{(1+h)R'(\sigma_+) + (1-h)R'(\sigma_-)}\right]^2\right\}\sigma^2. \tag{49}$$

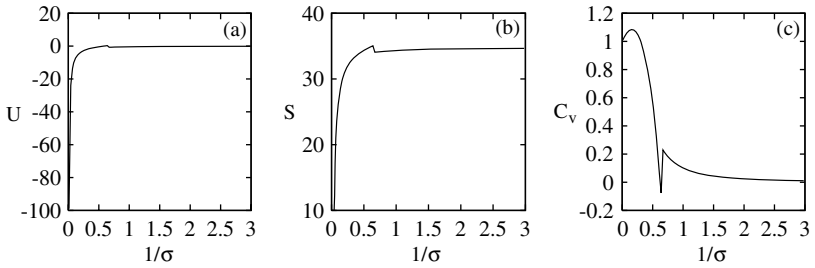

Figure 12. Temperature dependence of (a) u, (b) S and (c) specific heat for the zero field case.

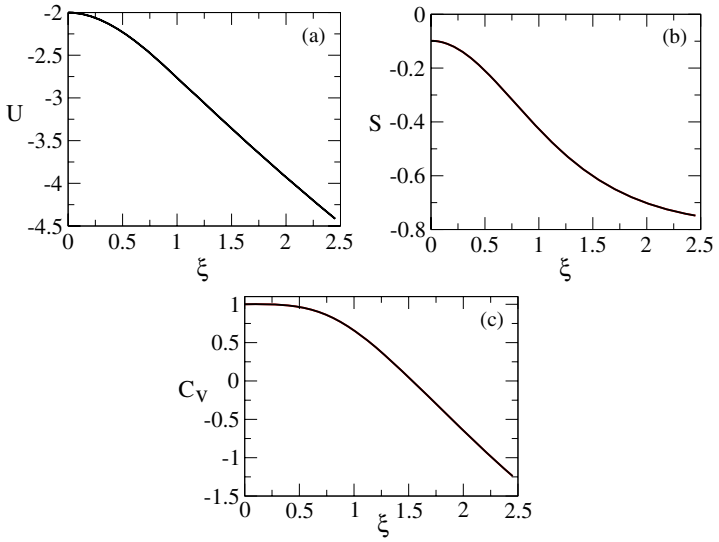

Figure 13. Inverse temperature dependence of (a) u, (b) S and (c) specific heat for the Ising case.

The temperature dependence for the different caloric quantities for various limiting cases are shown in figures 11, 12, 13, 14 and 15. In all the above mentioned limiting cases, specific heat obeys a T^{-2} law at high temperatures and tends to nonzero values at low temperatures. This last fact does not obey Nernst's theorem which states that $C_v \to 0$ as $T \to 0$. This actually occurs due to the classical nature of the spins. In the longitudinal field case, entropy and specific heat both display a maximum. The height and location of this maximum depend on the applied field. At high fields Zeeman energy dominates over the anisotropy energy and thus smears out the maximum and its height decreases. This maximum can be understood in terms of crossover from the high-temperature isotropic regime to the low temperature Ising regime.

5. Summary and conclusions

We have studied the magnetic and caloric properties of non-interacting anisotropic nanoparticles. Through the low-field expansion of magnetization, we derive linear (χ_0) and nonlinear susceptibilities (χ_2, χ_4) for a number of particular situations. In this analysis we have examined the effect of anisotropic potential on these magnetic properties of superparamagnetic

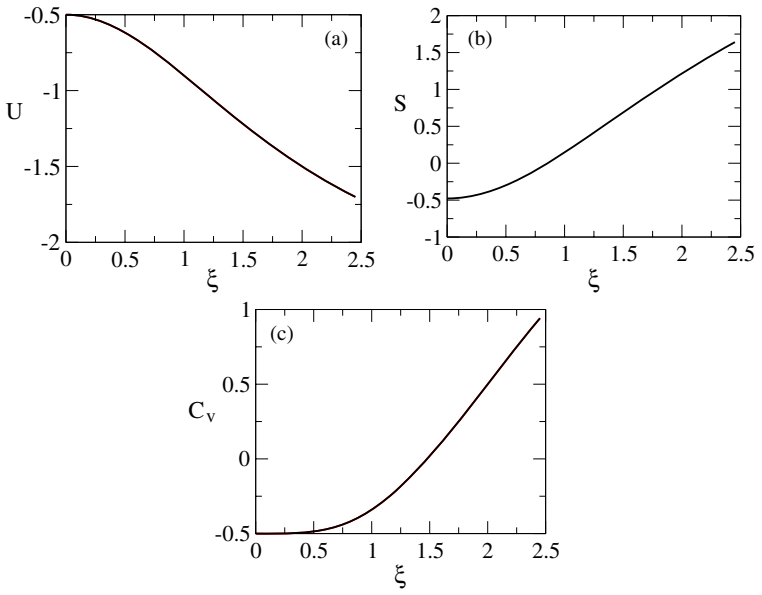

Figure 14. Inverse temperature dependence of (a) u, (b) S and (c) specific heat for the plane-rotator case.

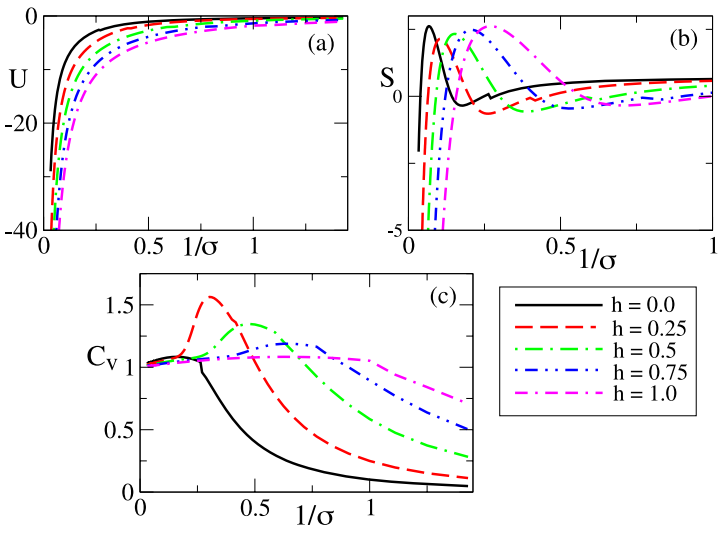

Figure 15. Temperature dependence of (a) u, (b) S and (c) specific heat for the longitudinal field case.

fine particles. This anisotropic potential induces a crossover from free-rotator to either the two-state or plane-rotator regime. In the crossover regime the temperature dependences of χ_0, χ_2 and χ_4 are much steeper than those of the limit inverse-temperature power laws (T^{-1}, T^{-3} and T^{-5}), respectively. This will misleadingly suggest interparticle interaction because the nonlinear susceptibilities will resemble the high-temperature ranges of divergence at low temperature. Thus we have drawn out the basic differences between the canonical spin-glass phase transition (e.g. in $Au_{96}Fe_4$) and the progressive freezing of the supermoments (e.g. in $Cu_{97}Co_3$). The linear susceptibility χ_0 and nonlinear susceptibility χ_4 show a positive peak whereas χ_2 has a negative peak for the superparamagnetic fine-particle systems. However, the negative peak in χ_2 and positive peaks in χ_0 and χ_4 are very broad compared with those of the spin-glass systems. The roundness of the peak and the width of the susceptibility curves

are marking features between the spin-glass phase transition and the progressive freezing of the supermoments. The analysis of the caloric properties shows the essential role of the anisotropic potential and it proves the classical nature of the supermoments.

The above analysis indicate that the origin of the magnetic properties of superparamagnetic fine particles and spin-glasses is very different, though the behaviour of linear susceptibility and the magnetization of fine particles is similar to those of spin-glasses. The nonlinear susceptibilities play a crucial role in distinguishing the canonical spin-glass phase transition and the progressive freezing of supermoments. In conclusion, we can say that our study will help to distinguish between the spin-glass transition and the progressive freezing of supermoments.

Acknowledgments

MB acknowledges financial support from the Council of Scientific and Industrial Research (CSIR), Government of India. JB acknowledges the Department of Science and Technology (DST), Government of India for the financial support.

References

[1] Neel L 1949 *Ann. Geophys.* **5** 99
[2] Dormann J L, Fiorani D and Tronc E 1997 *Adv. Chem. Phys.* **98** 283
[3] Puntes V F, Krishnan K M and Alivisatos A P 2001 *Science* **291** 2115
[4] Frankel J and Dorfman J 1930 *Nature* **126** 274
Kittel C 1946 *Phys. Rev.* **70** 965
[5] Sun S, Murray C B, Weller D, Folks L and Moser A 2000 *Science* **287** 1989
[6] Bean C P and Livingstone J D 1959 *J. Appl. Phys.* **30** 120s
Jacobs I S and Bean C P 1963 *Magnetism* vol III, ed G T Rado and H Suhl (New York: Academic)
[7] Aharoni A 1964 *Phys. Rev.* A **135** 447
Raikher Yu L and Shlimis M I 1974 *Zh. Eksp. Teor. Fiz.* **67** 1060
Raikher Yu L and Shlimis M I 1975 *Sov. Phys.—JETP* **40** 526
Kumar D and Dattagupta S 1983 *J. Phys. C: Solid State Phys.* **16** 3779
Coffey W T, Crothers D S F, Kalmykov Yu P, Massawe E S and Waldron J T 1994 *Phys. Rev.* E **49** 1869
[8] Raikher Yu L and Stepanov V I 1995 *Phys. Rev.* B **52** 3493
[9] Brown W F Jr 1963 *Phys. Rev.* **130** 1677
[10] Edwards S F and Anderson P W 1975 *J. Phys. F: Met. Phys.* **5** 965
[11] Dormann J L, Fiorani D, Tholence J L and Sella C 1983 *J. Magn. Magn. Mater.* **35** 117
[12] Fiorani D, Tholence J and Dormann J L 1986 *J. Phys. C: Solid State Phys.* **19** 5495
[13] Chantrell R W, El-Hilo M and O'Grady K 1991 *IEEE Trans. Magn.* **27** 3570
[14] El-Hilo M and O'Grady K 1988 *IEEE Trans. Magn.* **26** 1807
[15] El-Hilo M, O'Grady K and Popplewell J 1991 *J. Appl. Phys.* **69** 5133
[16] Dormann J L, Bessais J and Fiorani D 1988 *J. Phys. C: Solid State Phys.* **21** 2015
[17] Bitoh T, Ohba K, Takamatsu M, Shirane T and Chikazawa S 1993 *J. Phys. Soc. Japan* **62** 2583
Bitoh T, Shirane T and Chikazawa S 1993 *J. Phys. Soc. Japan* **62** 2837
[18] Jönsson T, Mattson J, Djurberg C, Khan F A, Nordblad P and Svedlindh P 1995 *Phys. Rev. Lett.* **75** 4138
[19] Garcia-Palacios J L and Lazaro F J 1997 *Phys. Rev.* B **55** 1006
Garcia-Palacios J L and Lazaro F J 1998 *Phys. Rev.* B **58** 14937
[20] Arfken G B and Weber H J 1997 *Mathematical Methods for Physicists* 5th edn (Boston, MA: Academic)
[21] Shih J W 1931 *Phys. Rev.* **38** 2051
[22] Cannella V and Mydosh J A 1974 *Phys. Rev.* B **6** 4220
[23] Lutes O S and Schmit J L 1964 *Phys. Rev.* **134** A676
[24] Bitoh T, Ohba K, Takamatsu M, Shirane T and Chikazawa S 1996 *J. Magn. Magn. Mater.* **154** 59
[25] Suzuki M 1977 *Prog. Theor. Phys.* **58** 1151
[26] Wada K and Takayama H 1980 *Prog. Theor. Phys.* **64** 327
[27] Sherrington D and Kirkpatrick S 1975 *Phys. Rev. Lett.* **35** 1752

J. Phys.: Condens. Matter **20** (2008) 219802 (1pp) doi:10.1088/0953-8984/20/21/219802

Erratum

Magnetic and caloric properties of magnetic nanoparticles: an equilibrium study

M Bandyopadhyay and J Bhattacharya
2006 *J. Phys.: Condens. Matter* **18** 11309

In the article 'Magnetic and caloric properties of magnetic nanoparticles: an equilibrium study', we discuss thermal equilibrium properties of non-interacting magnetically anisotropic nanoparticles. Some of the results related to χ_0, χ_2 and caloric properties are discussed earlier by J L García-Palacios in his classic article 'On the statics and dynamics of magneto-anisotropic nanoparticles' [1]. If someone is interested in this topic they should also consult the article of J L García-Palacios [1].

Reference

[1] J L García-Palacios 2000 *Advances in Chemical Physics* vol 112, ed I Priogogine and Stuart A Rice (New York: Wiley) 1

 © 2008 IOP Publishing Ltd Printed in the UK